

UC Davis

UC Davis Previously Published Works

Title

BRCA2 chaperones RAD51 to single molecules of RPA-coated ssDNA

Permalink

<https://escholarship.org/uc/item/77q319bj>

Journal

Proceedings of the National Academy of Sciences of the United States of America,
120(14)

ISSN

0027-8424

Authors

Bell, Jason C
Dombrowski, Christopher C
Plank, Jody L
et al.

Publication Date

2023-04-04

DOI

10.1073/pnas.2221971120

Peer reviewed



BRCA2 chaperones RAD51 to single molecules of RPA-coated ssDNA

Jason C. Bell^{a,b,1}, Christopher C. Dombrowski^{a,b,1}, Jody L. Plank^{a,b}, Ryan B. Jensen^{a,b,c}, and Stephen C. Kowalczykowski^{a,b,2}

Contributed by Stephen C. Kowalczykowski; received December 28, 2022; accepted February 24, 2023; reviewed by William K. Holloman and Scott W. Morrical

Mutations in the breast cancer susceptibility gene, *BRCA2*, greatly increase an individual's lifetime risk of developing breast and ovarian cancers. *BRCA2* suppresses tumor formation by potentiating DNA repair via homologous recombination. Central to recombination is the assembly of a RAD51 nucleoprotein filament, which forms on single-stranded DNA (ssDNA) generated at or near the site of chromosomal damage. However, replication protein-A (RPA) rapidly binds to and continuously sequesters this ssDNA, imposing a kinetic barrier to RAD51 filament assembly that suppresses unregulated recombination. Recombination mediator proteins—of which BRCA2 is the defining member in humans—alleviate this kinetic barrier to catalyze RAD51 filament formation. We combined microfluidics, microscopy, and micromanipulation to directly measure both the binding of full-length BRCA2 to—and the assembly of RAD51 filaments on—a region of RPA-coated ssDNA within individual DNA molecules designed to mimic a resected DNA lesion common in replication-coupled recombinational repair. We demonstrate that a dimer of RAD51 is minimally required for spontaneous nucleation; however, growth self-terminates below the diffraction limit. BRCA2 accelerates nucleation of RAD51 to a rate that approaches the rapid association of RAD51 to naked ssDNA, thereby overcoming the kinetic block imposed by RPA. Furthermore, BRCA2 eliminates the need for the rate-limiting nucleation of RAD51 by chaperoning a short preassembled RAD51 filament onto the ssDNA complexed with RPA. Therefore, BRCA2 regulates recombination by initiating RAD51 filament formation.

DNA recombination | DNA repair | breast cancer | RAD51 | single-molecule visualization

Mutations in the breast cancer susceptibility gene, *BRCA2*, greatly increase the lifetime risk of developing breast and ovarian cancers (1). *BRCA2* was identified in families with a high incidence of breast cancer (2). The relationship between BRCA2 and homologous recombination became evident when its interaction with RAD51 was discovered (3, 4). Cells lacking BRCA2 function suffer from genomic instability, loss of DNA damage-induced RAD51 foci, and extreme sensitivity to cross-linking agents such as mitomycin-C (MMC) and cisplatin (5–8). BRCA2 suppresses tumor formation by potentiating DNA repair via homologous recombination (6, 9–13).

As mentioned above, central to recombination is assembly of the RAD51 nucleoprotein filament onto ssDNA generated at the site of chromosomal damage. However, replication protein-A (RPA) rapidly binds to ssDNA, kinetically impeding RAD51 filament assembly. BRCA2, which is the defining member of recombination mediators in humans (9, 11, 14), alleviates this kinetic barrier to catalyze RAD51 filament formation (15, 16). Structurally, a unique feature of human BRCA2 is the presence of eight conserved BRC repeat sequences (3, 17, 18). Each BRC repeat binds RAD51 via an interface that mimics the RAD51 interface (3, 19–21). The carboxy-terminus of BRCA2 possesses three OB (oligonucleotide binding) folds with a tower structure protruding out of the second OB fold (22). This juxtaposition of DNA binding regions and the internal repeats necessary for RAD51 binding suggested a model whereby BRCA2 binds single-stranded DNA (ssDNA) or an ssDNA/dsDNA junction and loads RAD51 onto the ssDNA (23).

In vitro, full-length human BRCA2 promotes assembly of RAD51 onto ssDNA complexed with RPA, making it a bona fide mediator (9, 11, 24). BRCA2 binds to ssDNA with high affinity (~nM) in a structure-independent manner (i.e., an ssDNA–dsDNA junction is not required). BRCA2 also binds at least six monomers of RAD51, and likely up to eight, in a species-specific manner via its eight BRC repeats (9). The BRC repeats are neither identical in sequence nor in function. BRCA2 binds RAD51 through its eight BRC repeats in two distinct ways. BRC repeats 1 to 4 bind to free RAD51 with a high affinity and block both ssDNA-dependent Adenosine 5'-Triphosphate (ATP) hydrolysis and dsDNA binding (9, 20, 21). In contrast, BRC repeats 5 to 8 bind to and stabilize the

Significance

Despite decades of genetic and cell biological studies, mechanistic biochemical analyses of human BRCA2 function in recombinational DNA repair have only been possible since the purification of full-length BRCA2. These mechanistic studies crucially inform with respect to the molecular function of BRCA2 in genome maintenance. Here, we use single-molecule methods to visualize the assembly of RAD51 on individual molecules of single-stranded DNA (ssDNA) coated with replication protein-A (RPA) and to see how this process is regulated by the tumor suppressor protein, BRCA2. We show that BRCA2 serves as a chaperone to nucleate RAD51 and deliver it to RPA-coated ssDNA. This work advances understanding of the molecular functions of BRCA2 and, consequently, the molecular etiology of breast cancer in an important way.

Author contributions: J.C.B., C.C.D., J.L.P., R.B.J., and S.C.K. designed research; J.C.B. and C.C.D. performed research; J.C.B., C.C.D., J.L.P., and R.B.J. contributed new reagents/analytic tools; J.C.B., C.C.D., J.L.P., R.B.J., and S.C.K. analyzed data; and J.C.B. and S.C.K. wrote the paper.

Reviewers: W.K.H., Weill Cornell Medicine; and S.W.M., University of Vermont.

The authors declare no competing interest.

Copyright © 2023 the Author(s). Published by PNAS. This open access article is distributed under [Creative Commons Attribution License 4.0 \(CC BY\)](https://creativecommons.org/licenses/by/4.0/).

¹J.C.B. and C.C.D. contributed equally to this work.

²To whom correspondence may be addressed. Email: sckowalczykowski@ucdavis.edu.

This article contains supporting information online at <https://www.pnas.org/lookup/suppl/doi:10.1073/pnas.2221971120/-/DCSupplemental>.

Published March 28, 2023.

nascent RAD51-ssDNA filament to prevent disassembly (21, 25). BRC1-4 also blocks ATP hydrolysis by RAD51, which prevents dissociation of RAD51 from ssDNA and keeps RAD51 in the active ATP-bound form. This partitioning of labor suggested a mechanism where BRCA2 delivers up to four molecules of RAD51 to the ssDNA to serve as the nucleus to initiate assembly, and then the next four BRC repeats stabilize the next four molecules of RAD51 as they bind to ssDNA adding to the nucleus. In this way, BRCA2 was hypothesized to chaperone nascent filament assembly of eight RAD51 monomers, which comprises slightly more than one turn of the filament (~6 monomers).

In this work, we used optical trapping to physically manipulate single molecules of DNA that were engineered to contain a large ssDNA gap, mimicking a replication gap that is one of the several physiological substrates for the recombinational DNA repair. We incubated these gapped molecules with RPA and then, using optical trapping, we “dipped” each molecule into a solution containing RAD51 with, or without, purified BRCA2. By measuring the binding locations of each RAD51 and BRCA2, and the concentration

dependence of the kinetics of RAD51 nucleation on RPA-coated ssDNA, we ascertained that BRCA2 functions as a molecular chaperone for RAD51 to accelerate filament nucleation to overcome the kinetic inhibition imposed by RPA.

Results and Discussion

Using a microfluidic multichannel flow cell, coupled with a fluorescence microscope and a dual optical trap, two streptavidin-coated beads were isolated and a single molecule of DNA, biotinylated at each end, was tethered between the beads in situ (Fig. 1A, *illustration*) (15, 26–28). To image the assembly of RAD51 filaments on RPA-coated ssDNA, we used a dsDNA substrate containing an ssDNA gap of 8,155 nucleotides (nt) flanked by 21,080 bp and 24,590 bp of dsDNA (Fig. 1B) (28). To create this substrate, we used a derivative of bacteriophage λ gt11 containing a ϕ C31 *attP* recognition site and a derivative of bacteriophage M13mp7 ssDNA containing the *attB* sequence, which creates the duplex DNA recognition site upon annealing of a complementary DNA strand.

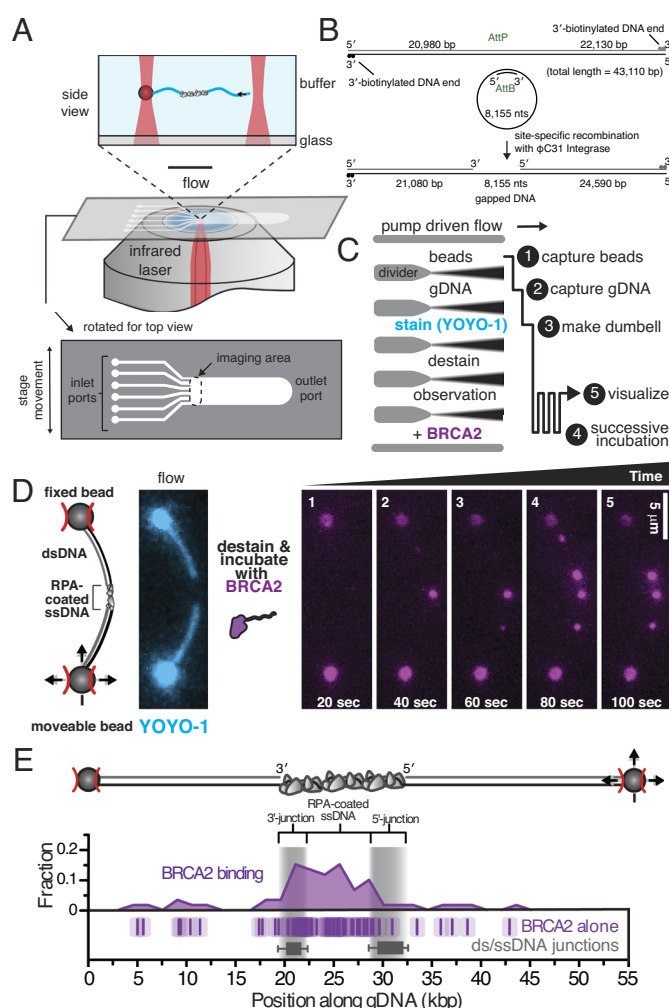


Fig. 1. Direct imaging of BRCA2 binding to RPA-coated ssDNA on single molecules of gapped λ DNA. (A) Schematic of experimental approach combining fluorescence microscopy, a microfluidic flow cell, and optical trapping, as well as the micromanipulation used to capture and image BRCA2 on individual DNA molecules. (B) Illustration of the gapped λ DNA generated through in vitro recombination of circular ssDNA with an engineered λ DNA. (C) Schematic of experimental protocol: Each molecule of gapped λ DNA was captured and micromanipulated between two beads held in separately controllable optical traps. The molecule was moved between solutions in a six-channel flow cell and successively incubated in a solution containing BRCA2. (D) Cartoon and microscopic image of a single molecule of gapped λ DNA (Left, stained with YOYO-1, cyan) that was destained and then successively incubated with BRCA2 (5 nM) plus α -BRCA2 and α -IgG^{AF546}. Montage shows BRCA2 (magenta) binding to the gapped λ DNA at increasing time intervals. (E) Cartoon representation of the gapped λ DNA between two beads (Top) and histogram (Middle) of binding positions of BRCA2 (number of foci, N = 60). Each data point is also plotted as a single tick (Bottom) where the semi-transparent box represents the SE associated with assigning position owing to the optical resolution of the microscope. Gray bars represent the 10 to 90th percentile range of the 5'- and 3'-terminated junctions (N = 98).

Integration of the circular ssDNA into biotinylated λ DNA resulted in a DNA substrate that we hereafter refer to as gapped λ DNA. This substrate mimics a replication gap—one of the primary lesions requiring recombination-coupled DNA repair in normal cell division—arising from incomplete lagging strand synthesis or resection from a replication block. Unless specifically indicated, the gapped λ DNA was preincubated with purified human RPA before capture in the optical traps, and RPA was present in each channel of the flow cell to ensure that ssDNA within the gap would be entirely coated with RPA.

Each isolated molecule was first visualized using YOYO-1 to stain the dsDNA portions, so as to establish the integrity and orientation of each molecule. YOYO-1 was then dissociated by incubation in the “destain” channel, and each molecule was then successively incubated in a channel containing full-length human BRCA2 [purified as previously described (9)], and visualized by coincubation with a fluorescently labeled antibody (Fig. 1C). Each molecule was rotated perpendicular to the flow to maximize spatial resolution, while minimizing flow-exerted forces on the RPA-coated ssDNA. With time, BRCA2 binding was directly observed along the DNA (Fig. 1D and Movie S1); the variation in intensity likely results from the heterogeneous nature of the fluorescently labeled antibody used for detection or possibly the presence of multimeric forms of BRCA2 (29). The initial position of each binding event was determined by measuring the relative distance of each fluorescent focus along the contour length of the DNA between the beads. Due to intercalation of YOYO-1 into dsDNA, the contour length of the molecule changes after YOYO-1 dissociation but we could determine the orientation of each molecule and the position of each binding event relative to the ssDNA–dsDNA junctions, which is plotted in Fig. 1E. In aggregate, BRCA2 binding demonstrated a preference for binding the ssDNA region, despite the presence of RPA, consistent with our previous observation that BRCA2 preferentially binds ssDNA over dsDNA². Binding events observed on dsDNA were more labile, and infrequently, molecules of BRCA2 bound to dsDNA under flow were observed sliding on the dsDNA (Movie S1 and SI Appendix, Fig. S1).

To visualize the formation of a RAD51 filament, we attached gapped λ DNA to the surface of a PEG-coated flow cell and initially used total internal reflection fluorescence (TIRF) microscopy (Fig. 2B), taking advantage of the higher throughput of TIRF experiments (28). The dsDNA region of the molecule was imaged using SYTOX Orange. The ssDNA gap was clearly visible owing to the absence of SYTOX Orange staining. When purified fluorescent RAD51 (previously described) (30) was injected into the flow

cell, the RAD51-binding buffer caused dissociation of the SYTOX Orange from the dsDNA within 1 to 3 s and, with time, RAD51 filaments formed on the ssDNA region. In the absence of RPA, association of RAD51 was almost as fast as we could measure: The lag time for nucleation—determined as the time for detection of the first diffraction-limited focus on the ssDNA—was on the order of 5 to 10 s, and binding was complete after 1 to 2 min (Fig. 2B and Movie S2). In contrast, when RPA was included, RAD51 filament formation was potentially blocked (Fig. 2C): in this example, nucleation was not evident until 120 s and complete filaments (ascertained by “filling in” of the gap) were not observed even at 240 s (Fig. 2C and Movie S3), after which some photobleaching is apparent. It is worth noting that previous single-molecule experiments demonstrated the binding of RAD51 to dsDNA in the absence of salt; however, this off-target binding is dramatically reduced between 150 and 300 mM NaCl (30), the range of ionic strength physiologically relevant for the mammalian nucleus (31). Therefore, all RAD51 binding experiments were performed in 200 mM NaCl (Materials and Methods).

We next measured the times for RAD51 nucleation in the absence and presence of RPA. On average, nucleation of RAD51 in the absence of RPA was fast, limited primarily by the dead time of the injection of fluorescent RAD51 into our flow cell, with an average lag time of 5 ± 3 s (Fig. 2D, Leftmost). In the presence of RPA, the nucleation time slowed by 16-fold, with an average lag time of 78 ± 40 s (Fig. 2D, Center). The lag times obtained from our TIRF and trapping assays were identical, within error (SI Appendix, Fig. S2); however, we elected to use the optical trapping assay for further experiments containing BRCA2 owing to the smaller volumes and lower flow rates, which greatly reduced the material required for each experiment. When we measured the nucleation time for RAD51 in the presence of BRCA2, we observed a threefold to fourfold net reduction from 78 ± 40 s in the absence of BRCA2, to 27 ± 11 s in the presence of BRCA2 (Fig. 2D, Rightmost) which approaches, within a factor of four, the nucleation rate observed when RPA is absent.

We subsequently visualized RAD51 nucleation on gapped λ DNA using two-color fluorescence microscopy (Fig. 3A, schematic), to simultaneously image both RAD51 nucleation and BRCA2 binding (Fig. 3B). Fig. 3B shows two distinct nucleation events, where one event (the focus on the top, colocalized with BRCA2, which is yellow in the merged image) is mediated by BRCA2, whereas the second nucleation event (green in the merged image) is a spontaneous nucleation event. These experiments also confirmed the expected colocalization of RAD51 and BRCA2 in 56% of these RAD51 nucleation

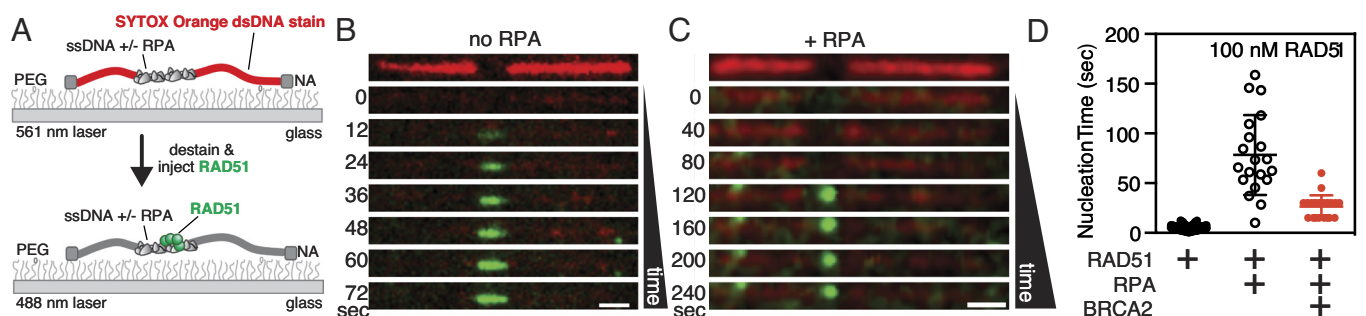


Fig. 2. Direct imaging of RAD51 nucleation and filament formation in the absence and presence of RPA. (A) Schematic of a single molecule of gapped λ DNA attached at each end to a PEG-coated surface via neutravidin. The dsDNA region was initially visualized using SYTOX Orange (red), which was subsequently dissociated upon the addition of binding buffer and fluorescein-RAD51 (green). (B) In the absence of RPA, fluorescent RAD51 rapidly filled the ssDNA region. (C) When RPA was present, RAD51 binding was slower and punctate. (D) Comparison of the lag time in the absence (black filled symbols) or presence (black open symbols) of RPA measured using TIRF microscopy. Lag times in the presence of BRCA2 were measured using optical trapping (see text) and are shown in red symbols for comparison. Lines represent the arithmetic mean and error bars represent SD. No RPA: 5 ± 3 ($N = 111$); +RPA: 78 ± 40 ($N = 20$); +RPA/BRCA2: 27 ± 11 ($N = 22$). (Scale bar in panels B and C is 2 μ m.)

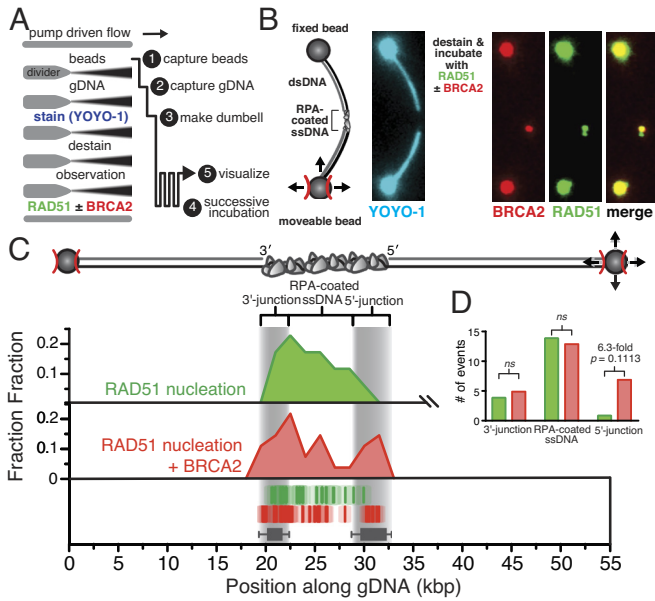


Fig. 3. RAD51-BRCA2 complexes, in contrast to BRCA2 alone, are focused to the ssDNA regions. (A) Schematic of optical-trap experiments designed to visualize nucleation of RAD51 on gapped λ DNA in the absence or presence of BRCA2. (B) A single molecule of gapped λ DNA with bound RPA held between two optical traps and cocubated with 100 nM RAD51 (green) and 5 nM BRCA2 (red, α -MBP^{AF546}). (C) Cartoon of the gapped λ DNA (Top) and histogram (Middle) showing positions of all RAD51 nucleation events either alone (green) ($N = 18$) or when coincubated with BRCA2 (red) in the absence of antibody ($N = 28$). Positions of individual foci are plotted (Bottom) relative to position of the 5'- and 3'-terminated junctions. The transparent box around each dash represents the SE owing to the optical resolution of our microscope. Gray bars represent the 10 to 90th percentile range of the 5'- and 3'-terminated junctions ($N = 98$). (D) Bar plot of the number of RAD51 nucleation events in the absence (green) or presence of BRCA2 (red) observed in the regions nearest the 3'-junction, clearly in the middle of the RPA-coated region, or near the 5'-junction. The odds ratios and P -values were calculated using Fisher's exact test.

events, slightly more than the 40% expected due to the ~ 2.5 -fold excess of RAD51 over binding sites on BRCA2. As previously described for Fig. 1, we measured the position of each nascent RAD51 filament relative to the junctions along the gapped λ DNA and plotted every position observed for the duration of the imaging protocol (Fig. 3C), in either the absence (green) or presence (red) of BRCA2 in the absence of antibody so as not to potentially alter the outcome. RAD51 nucleation was exclusively observed within the RPA-coated ssDNA region, with usually one RAD51 focus per DNA molecule and generally no more than three. There was an apparent skewed preference (Fig. 3D) for the ssDNA region near the 3'-terminated junction relative to the 5'-junction (odds ratio = 4.7, $P = 0.3377$; Fisher's exact test). In the presence of BRCA2, we observed a 6.3-fold increase in the number of nucleation events near the 5'-terminated junction relative to the RAD51-alone condition (odds ratio = 6.3, $P = 0.1113$; Fisher's exact test), resulting in nascent RAD51 foci forming closer to the edges of the RPA-coated ssDNA region, consistent with both the twofold higher affinity for ssDNA-dsDNA junctions established from ensemble studies (9) and a potential kinetic bias resulting from BRCA2 sliding down the dsDNA under flow.

We next analyzed the kinetics of RAD51 nucleation on RPA-coated ssDNA as a function of RAD51 concentration, plotting the cumulative frequency of RAD51 nucleation events as a function of increasing incubation time (Fig. 4A and B). When analyzed in this way, the observed cumulative frequency increases exponentially with time, and a characteristic nucleation time can be determined by fitting the data to a single exponential curve. As expected, the nucleation time decreased as the concentration of RAD51 increased. In the absence of BRCA2 (Fig. 4A),

spontaneous nucleation is strongly dependent on the concentration of RAD51, where the rate of nucleation is proportional to the concentration of the filament-forming protein raised to the power of the minimum nucleation species (i.e., $J \propto k \cdot [\text{RAD51}]^n$, where $J = 1/\text{lag time}$, n is the size of the oligomer, and k is a dimensionless rate constant) (28, 30, 32, 33). Using this kinetic analysis, we observed a power dependence where $n = 1.5 \pm 0.3$ (Fig. 4C), indicating that RAD51 nucleation proceeds through either monomers or dimers; however, since RAD51 nucleation is nucleotide dependent and the nucleotide-binding interface lies between two half sites formed between adjacent monomers, we conclude that in the absence of BRCA2, the smallest oligomer required for a single nucleation event on RPA-coated ssDNA is a dimer of RAD51, similar to previous observations with both RecA (28) and RAD51 in the absence of RPA (30, 33).

When we repeated the experiment in the presence of BRCA2, the RAD51 nucleation times were decreased (Fig. 4B), as anticipated. Unexpectedly, the kinetics of RAD51 nucleation were independent of RAD51 concentration across the accessible range of our assay (Fig. 4C). To determine whether the time to RAD51 nucleation was strictly limited by the kinetics of BRCA2 binding to the ssDNA coated with RPA, we measured the kinetics of BRCA2 binding to RPA-coated ssDNA in the absence of RAD51 as shown in Fig. 1D, and plotted the data (Fig. 4B, blue open circles & dashed line, BRCA2 only). The binding of BRCA2 in the absence of RAD51 exhibits a sigmoidal increase with a characteristic half-time of ~ 25 s. In contrast, nucleation of RAD51 in the presence of BRCA2 was \sim twofold faster than binding of BRCA2 alone (Fig. 4C, purple), with a characteristic half-time of 7 to 12 s and was independent of the concentration of RAD51 (Fig. 4C, red). The faster rate of DNA binding for BRCA2 in the presence of RAD51 indicates that the proteins bind as a complex, consistent with the role of BRCA2 functioning as a molecular chaperone to promote RAD51 nucleation. The conclusion is quantitatively substantiated by the data in Fig. 4C which reveal that BRCA2 eliminates the apparent concentration dependence of RAD51 nucleation, demonstrating that RAD51 is delivered by BRCA2 to the ssDNA in a prenucleated form and bypassing the otherwise rate-limiting step of dimer formation during filament assembly.

Our observations advance a model whereby BRCA2 functions to chaperone RAD51 to RPA-coated ssDNA during recombination-mediated DNA repair to promote nucleation of a RAD51 filament. Our single-molecule imaging of RAD51 filament assembly on its in vivo substrate, RPA-coated ssDNA, establishes that a dimer of RAD51 is minimally required for nucleation followed by slow and self-terminating growth. When bound to ssDNA, RPA is a potent and persistent kinetic block to RAD51 binding. The tumor suppressor protein, BRCA2, overcomes this kinetic block by accelerating RAD51 nucleation to rates approaching those seen on ssDNA devoid of RPA. We propose that BRCA2 achieves this task by delivering, via its BRC repeats, a preassembled nucleus of RAD51 directly to the DNA. We imagine that the eight BRC repeats of BRCA2 organize RAD51 monomers into a prefilament that could comprise a nucleus of up to four monomers bound to BRC1-4; the number of BRC repeats is clearly overspecified, as only one BRC in the *Ustilago maydis* Brh2 homolog or in heterologous protein fusions is minimally required for recombinational repair (34, 35). BRCA2 could also potentially recruit four more monomers via BRC5-8 when the BRCA2-RAD51 complex binds to ssDNA (21). The result would be a nascent RAD51 filament of up to eight monomers—more than one turn of the filament—sembled by the chaperoning capacity of BRCA2. Consistently, other single-molecule observations revealed stable nuclei or nascent filaments ranging in size from 2 to 10 RAD51 monomers, with a stability that increased with length

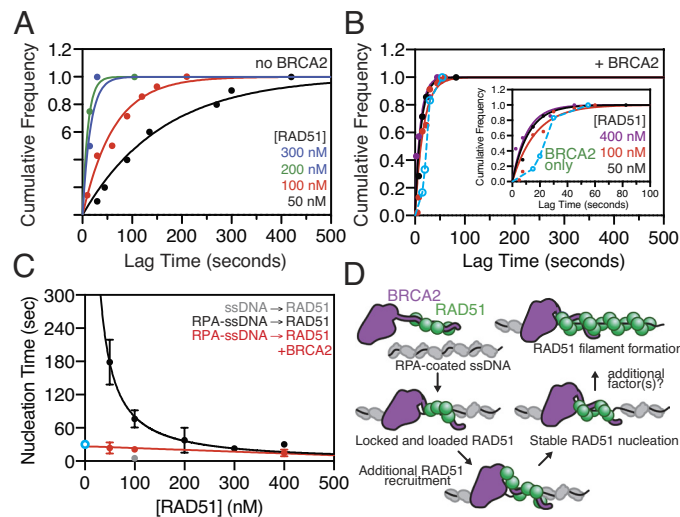


Fig. 4. Nucleation of RAD51 requires a dimer and is accelerated by BRCA2 by delivering a pre-nucleated complex. (A) The cumulative frequency of RAD51 nucleation measured by optical trapping is plotted as a function of increasing incubation time at varying concentrations of RAD51 in the absence or (B) presence of BRCA2. *Inset* shows a zoomed-in scale. The solid lines represent nonlinear fitting to a single-exponential rate equation: 50 nM: $t_{1/2} = 110 \pm 10$ s, 100 nM: $t_{1/2} = 47 \pm 4$ s, 200 nM: $t_{1/2} = 8 \pm 1$ s, 300 nM: $t_{1/2} = 11 \pm 4$ s (SE). The open symbols and cyan dashed line represent the kinetics of BRCA2 binding in the absence of RAD51 as measured in Fig. 1 and is shown as a comparison to the kinetics of RAD51 nucleation (see text). (C) The arithmetic mean nucleation time plotted as a function of increasing RAD51 concentration in the absence: 50 nM: 179 ± 41 s ($N = 10$), 100 nM: 76 ± 16 s ($N = 14$), 200 nM: 38 ± 23 s ($N = 4$), 300 nM: 23 ± 4 s ($N = 4$), 400 nM: 30 ± 6 s ($N = 6$), or presence of BRCA2: 50 nM: 24 ± 10 s ($N = 7$), 100 nM: 21 ± 2 s ($N = 46$), 400 nM: 15 ± 6 s ($N = 7$). The black curve represents a fit to the power law ($f = k[\text{RAD51}]^n$) where $n = 1.5 \pm 0.3$ (SE). The cyan symbol represents the half-time for BRCA2 binding in the absence of RAD51, measured with α -BRCA2 plus α -IgG^{AF546}: 30 ± 6 s ($N = 6$). The red line is for visual purposes only; gray symbol is the rate in the absence of RPA: 5.2 ± 0.3 s ($N = 111$). Error and error bars are SEM, and if not visible, are smaller than the symbol. (D) Model of BRCA2-mediated RAD51 nucleation on RPA-coated ssDNA.

(33). Hence, even though 1 BRC may suffice to recruit a dimer of RAD51, as in the case of RecA loading by RecBCD enzyme (36), the presence of eight BRC repeats may ensure the highest stability of a nascent RAD51 filament. Nonetheless, the specific coordination between the BRC repeats remains to be elucidated. Interestingly, in our experiments containing RPA, RAD51 filaments were restricted to diffraction-limited foci, in contrast to the contiguous structures that form on the ssDNA region in the absence of RPA. This leads us to conclude that, under the conditions of our assay, BRCA2 can facilitate RAD51 nucleation onto RPA-bound ssDNA but it is not capable of stimulating growth of the RAD51 filament beyond spatial limitation of our measurement (~0.6 kb). *In vivo*, the amount of ssDNA generated following resection or replication fork gap repair may only require a limited stretch (200 to 300 nt) of RAD51 filament formation to promote strand invasion and homology-directed repair (37). Alternatively, other recombination mediators could assist during the growth phase to further extend RAD51 filaments along regions of ssDNA (15, 16, 38). In *Escherichia coli*, the functional analogs of BRCA2 are RecF, RecO, and RecR, which function as a modular set of protein complexes (RecOR and RecFOR), where RecOR stimulates both nucleation and growth of RecA filaments by remodeling the SSB-ssDNA complex, and RecFOR promotes nucleation at or near the ssDNA-dsDNA junctions (28, 39). BRCA2 enhances nucleation of RAD51 filaments, but an as yet-to-be-determined mediator supports RAD51 growth potentially by remodeling RPA-ssDNA structures. Genetically, the RAD51 paralogs are epistatic to BRCA2 (40, 41) and are likely candidates for such a role. Further exploration of this hypothesis awaits more complete biochemical characterization of functionally active human RAD51 paralogs.

Materials and Methods

Single-Molecule Measurements. For TIRF imaging, all protein-containing reagents were diluted into single-molecule buffer containing 20 mM TrisOAc (pH 7.5), 50 mM dithiothreitol (DTT), 20% sucrose, 200 mM NaCl, 2 mM CaCl₂, 1 mM Mg(OAc)₂, 1 mM ATP, and 100 nM RPA, unless otherwise indicated. The

glass surface was cleaned with Piranha solution (7.5% hydrogen peroxide in concentrated sulfuric acid) and functionalized using biotin-PEG silane and blocked. The gapped DNA substrate (gKytos, ~5 pM molecules) was biotinylated at both ends and attached to the surface *in situ* by alternating the flow off and on using a computer-controlled syringe pump at a flow rate of 4 mL per hour. SYTOX Orange, a dsDNA-specific stain, was used to visualize the dsDNA-regions of the gapped DNA molecules. Owing to the presence of salt and divalent cation, SYTOX Orange dissociated from the dsDNA, causing a decrease and eventually disappearance of fluorescence signal. The kinetics of RAD51 nucleation were then observed by injecting 100 nM fluorescent RAD51 [N-terminal linkage with fluorescein, previously described (30)] in the absence or presence of 5 nM 2 \times -MBP-tagged BRCA2 [purified as previously described (9)].

Epi-fluorescent trapping experiments were performed using a six-channel laminar flow cell. The channels contained the following components, in addition to 20% sucrose and 50 mM DTT: **(Ch 1)** 100 mM NaHCO₃ (pH 8.3), 100 mM NaCl, 1 mM Mg(OAc)₂, 5 nM YOYO-1, and 0.2% streptavidin-coated polystyrene beads (1 μ m, Bangs); **(Ch 2)** 100 mM NaHCO₃ (pH 8.3), 100 mM NaCl, 1 mM Mg(OAc)₂, 50 nM YOYO-1, 2 pM gapped DNA, and 200 nM RPA; **(Ch 3)** 100 mM NaHCO₃ (pH 8.3), 100 mM NaCl, 1 mM Mg(OAc)₂, 50 nM YOYO-1, and 50 nM RPA; **(Ch 4)** 100 mM NaHCO₃ (pH 8.3) and 50 nM RPA; **(Ch 5)** 20 mM Tris(OAc) (pH 7.5), 200 mM NaCl, 2 mM CaCl₂, 1 mM Mg(OAc)₂, 1 mM ATP, and 50 nM RPA; and **(Ch 6)** 20 mM Tris(OAc) (pH 7.5), 200 mM NaCl, 2 mM CaCl₂, 1 mM Mg(OAc)₂, 1 mM ATP, 50 nM RPA, and 100 nM fluorescent RAD51, unless otherwise indicated. When present, BRCA2 was at 5 nM. Experiments designed to visualize BRCA2 binding, either in the presence or absence of fluorescent RAD51, also contained 1 to 2 μ g/ μ L α -MBP^{AF546} or 1 to 2 μ g/ μ L mouse α -BRCA2 (Ab1, Millipore) plus 1 to 2 μ g/ μ L goat α -mouse IgG^{AF546} (Molecular Probes).

Total Internal Reflection Fluorescence Microscopy and Single-Channel Flow Cells. An Eclipse TE2000-U, inverted TIRF microscope (Nikon), using a CFI Plan Apo TIRF 100 \times , 1.49 N.A., oil-immersion objective, was used as previously described (27, 28). Single-channel flow cells were constructed by drilling holes into a glass microscope slide and adhering a cover glass using 3M Thermo-Bond Film (2.5 ml) with a channel cut out from the tape of dimensions (5 mm \times 35 mm \times 0.1 mm). Inlet ports (PEEK tubing, 0.5 mm inner diameter) were attached to the flow cell using epoxy (Devcon, "5 min"). The cover glass (Fisher's *Finest*, 22 \times 50 #1) was cleaned by submersion in Piranha solution (one volume 30% hydrogen peroxide slowly mixed with four volumes of concentrated sulfuric acid) for 15 to 30 min. The cover glass was rinsed with water and then methanol, then sonicated

in a solution of 1 M KOH dissolved in methanol for 1 h or soaked overnight without sonication. The cover glass was then rinsed with water and methanol, dried under a stream of nitrogen, and then arranged on a slide heater set to 70 °C. The surface was functionalized with 330 μL per cover glass ($\sim 0.3 \mu\text{L}$ per mm^2) of mPEG-5000-silane (5 mg/mL, Laysan Bio) and biotin-PEG-5000 silane (5 $\mu\text{g}/\text{mL}$, Laysan Bio) dissolved in 0.5 N HCl and 80% ethanol. After the solution evaporated, the top half of a bell-shaped vacuum chamber was placed over the cover glass on the heater and the surface was cured overnight at 70 °C under vacuum. The next day, the cover glass was rinsed with water, dried under stream of nitrogen, and stored either in a vacuum chamber or in jar purged with nitrogen for up to 2 wk. Flow cells were assembled using the double-sided tape with the cut channel. The surface was functionalized by incubating the flow cell successively with the following solutions for 5 to 10 min each: 1) buffer STE (20 mM TrisHCl (pH 7.5), 0.5 mM ethylenediaminetetraacetic acid (EDTA), and 200 mM NaCl) containing 0.2 mg/mL neutravidin; 2) rinsed with SMB (20 mM TrisOAc (pH 7.5), 50 mM DTT, and 20% sucrose); 3) blocked with SMB plus 1.5 mg/mL Roche Blocking Reagent and 2 mg/mL poly-glutamic acid (1,500 to 5,500 Da., Sigma-Aldrich); and then 4) rinsed with SMB. The gapped DNA substrate (gKytos, $\sim 5 \text{ pM}$ molecules) was biotinylated at both ends (see next section) and attached to the surface in situ by alternating the flow off and on using a computer-controlled syringe pump at a flow rate of 4 mL per hour. The dsDNA was visualized by the addition of 200 nM SYTOX Orange (Thermo Fisher).

Preparation of Gapped λ DNA. An engineered derivative of bacteriophage λ gt11 containing a ϕ C31 *attP* recognition site was created as previously described (28), and is hereafter called bacteriophage λ Kytos. Biotin was incorporated into the *cos* sites of λ Kytos in a reaction consisting of 10 mM Tris-HCl (pH 7.9), 10 mM MgCl_2 , 50 mM NaCl, 1 mM DTT, 33 μM dATP, 33 μM dTTP, 33 μM dCTP, 33 μM biotin-dGTP, 17 ng/ μL λ Kytos, and 0.17 U/ μL Klenow *exo*⁻ DNA polymerase. After 15 min at 22 °C, the polymerase was heat inactivated at 70 °C for 20 min and the DNA was purified by passing through an S-400 desalting spin column (GE Illustra Microspin). A modified derivative of bacteriophage M13mp7 ssDNA contained the *attB* recognition site, from which a 500 bp dsDNA containing the ϕ C31 *attB* at its center was generated by PCR using Phusion High Fidelity PCR Master Mix from New England Biolabs (NEB). After heat denaturation, it was annealed to the M13mp7 ssDNA derivative. ϕ C31 integrase was used to recombine λ Kytos dsDNA and the annealed 13mp7 ssDNA containing the *attB* recognition site. The construct pHS62, containing the full coding sequence of ϕ C31 integrase, was kindly provided by Margaret Smith (42). Integration of the ssDNA plasmid into λ Kytos dsDNA resulted in a gapped λ DNA substrate. The gapped λ DNA was purified in situ away from nonintegrated circular ssDNA either by attaching the molecules to the biotinylated polyethylene glycol (PEG) surface for TIRF microscopy, or by attaching the molecules to streptavidin-coated beads during optical trapping experiments.

Epifluorescence Microscopy, Optical Trapping, and Multichannel Flow Cells. Optical trapping was achieved on the same TE-2000-U microscope (Nikon) used for the TIRF-based assays. A polarizer (Newport) was used to split the beam from an infrared laser (Spectra-Physics), generating two traps, and a steering mirror (Newport) to control the x-y position of one of the beams (27, 28). Excitation of the sample in epifluorescence mode was achieved using a Cyan 488 nm laser (Picarro) by adjusting the angle of the laser to pass completely through the sample chamber. The fluorescence emission was directed through a dichroic mirror (515/30 nm and 600/40 nm, Chroma). Images were captured on a DU-897E iXon EMCCD camera (Andor). Custom flow cells were constructed as previously described (26, 43). Briefly, the flow cell design (Fig. 1A) was laser-etched into glass slides (Fisher Scientific 25 \times 75 \times 1 mm) covered with an adhesive abrasive blasting mask (Rayzist Photomask, Inc.) using a 30-Watt Mini-24 Laser Engraver (Epilog Lasers).

The slides were sandblasted using 220 grit silicon carbide (Electro Abrasives) to remove residual laser-ablated glass from the channels, resulting in channels ~ 100 to 150 μm deep and 850 μm wide (the total width of the six-channel flow cell was 5.1 mm). Holes were drilled using a diamond-coated bit and a Dremel hand-held drilling tool, washed with 2% Hellmanex III, and rinsed with water and methanol. The cover glass (Corning No. 1, 24 \times 60 mm) was cleaned in 1 M KOH/MeOH with sonication for 1 h, rinsed with water and methanol, and dried. The cleaned cover glass was attached to the etched microscope slide with UV Optical adhesive #74 (Norland Products) applied through capillary action on a 45 °C heat block. The adhesive was cured by placing the flow cell 30 cm from a 100-Watt HBO lamp (Zeiss, Inc.) for 60 min followed by curing at 50 °C overnight. polyetheretherketone (PEEK) tubing with 0.5 mm inner diameter (Upchurch Scientific) was inserted into each of the etched holes to create inlet and outlet connection ports and sealed with epoxy (Devcon, "5 min"). The flow cell was mounted to the microscope and attached to a computer-controlled syringe pump (KD Scientific). The temperature of the objective lens was held at 37 °C by circulating water through a brass and copper collar, machined to fit around the objective lens.

Once DNA dumbbells were assembled, imaging and incubations were performed in the center of the designated channel approximately 100 to 400 μm downstream of the channel dividers. Experiments designed to visualize BRCA2 binding, either in the presence or absence of fluorescent RAD51, contained 1.5 $\mu\text{g}/\text{mL}$ α -MBP^{AF546} (Abcam, labeled with Alexa Fluor 546, Molecular Probes) or 1.5 $\mu\text{g}/\text{mL}$ mouse α -BRCA2 (Ab-1, Millipore) plus 1-2 $\mu\text{g}/\text{mL}$ goat α -mouse IgG^{AF546} (Molecular Probes) as indicated in the figure legends. Sterile 0.2 μm filtered sucrose solutions were degassed for at least 1 h but typically overnight in a vacuum chamber before the addition of 50 \times buffer and DTT powder, then degassed for an additional 15 min; reactions were assembled at room temperature protected from light. Optically trapped molecules were moved between flow channels by movement of the sample stage, which was automated and synchronized with both laser excitation and camera acquisition during dipping experiments using software coded in LabView. Gapped λ DNA molecules containing fluorescent RAD51 filaments were successively transferred from Ch 6 to Ch 5, imaged for 1 s, and immediately transferred back to Ch 6. The time at which a RAD51 cluster first appeared was determined to be the apparent nucleation lag time. Images were processed in ImageJ by frame averaging, background subtraction, and contrast enhancement. Data were analyzed and plotted using GraphPad Prism (v7.0c). Fisher's exact test was computed using R-Studio (v 0.99.893).

Data, Materials, and Software Availability. All study data are included in the article and/or [supporting information](#).

ACKNOWLEDGMENTS. We would like to thank all the members of the Kowalczykowski lab for insightful comments and discussion. J.C.B. was supported in part by the National Institutes of Health - University of California Davis (NIH-UCD) Training Fellowship in Molecular and Cell Biology (T32 GM007377). C.C.D. and J.L.P. were supported by the NIH-UCD T32 Training Program in Oncogenic Signals and Chromosome Biology (CA10052159). J.L.P. was also supported by the NIH F32 Ruth L. Kirschstein National Research Service Award (CA136103). R.B.J. was supported by the American Cancer Society (#IRG 58-012-55); Breast Cancer Alliance; Pilot Project Program grant from Women's Health Research at Yale; the Yale Comprehensive Cancer Center; and a Liz Tilberis Early Career Award from the Ovarian Cancer Research Fund Alliance. S.C.K. was supported by NIH (GM62653, GM64745, and R35 GM131900) and DOD-CDMRP (BC171869).

Author affiliations: ^aDepartment of Microbiology and Molecular Genetics, University of California, Davis, CA 95616; ^bDepartment of Molecular and Cellular Biology, University of California, Davis, CA 95616; and ^cDepartment of Therapeutic Radiology, Yale University School of Medicine, New Haven, CT 06520

1. R. Wooster *et al.*, Identification of the breast cancer susceptibility gene BRCA2. *Nature* **378**, 789-792 (1995).
2. R. Wooster *et al.*, Localization of a breast cancer susceptibility gene, BRCA2, to chromosome 13q12-13. *Science* **265**, 2088-2090 (1994).
3. A. K. Wong, R. Pero, P. A. Ormonde, S. V. Tavtigian, P. L. Bartel, RAD51 interacts with the evolutionarily conserved BRC motifs in the human breast cancer susceptibility gene *brca2*. *J. Biol. Chem.* **272**, 31941-31944 (1997).
4. S. K. Sharan *et al.*, Embryonic lethality and radiation hypersensitivity mediated by Rad51 in mice lacking Brca2. *Nature* **386**, 804-810 (1997).

5. V. P. Yu *et al.*, Gross chromosomal rearrangements and genetic exchange between nonhomologous chromosomes following BRCA2 inactivation. *Genes. Dev.* **14**, 1400-1406 (2000).
6. M. E. Moynahan, A. J. Pierce, M. Jasin, BRCA2 is required for homology-directed repair of chromosomal breaks. *Mol. Cell* **7**, 263-272 (2001).
7. S. S. Yuan *et al.*, BRCA2 is required for ionizing radiation-induced assembly of Rad51 complex in vivo. *Cancer Res.* **59**, 3547-3551 (1999).
8. B. C. Godthelp, F. Artwert, H. Joenje, M. Z. Zdzienicka, Impaired DNA damage-induced nuclear Rad51 foci formation uniquely characterizes Fanconi anemia group D1. *Oncogene* **21**, 5002-5005 (2002).

9. R. B. Jensen, A. Carreira, S. C. Kowalczykowski, Purified human BRCA2 stimulates RAD51-mediated recombination. *Nature* **467**, 678–683 (2010).
10. P. L. Welch, K. N. Owens, M. C. King, Insights into the functions of BRCA1 and BRCA2. *Trends Genet.* **16**, 69–74 (2000).
11. J. Liu, T. Doty, B. Gibson, W. D. Heyer, Human BRCA2 protein promotes RAD51 filament formation on RPA-covered single-stranded DNA. *Nat. Struct. Mol. Biol.* **17**, 1260–1262 (2010).
12. T. Thorslund *et al.*, The breast cancer tumor suppressor BRCA2 promotes the specific targeting of RAD51 to single-stranded DNA. *Nat. Struct. Mol. Biol.* **17**, 1263–1265 (2010).
13. R. Prakash, Y. Zhang, W. Feng, M. Jasin, Homologous recombination and human health: The roles of BRCA1, BRCA2, and associated proteins. *Cold Spring Harb. Perspect. Biol.* **7**, a016600 (2015).
14. A. Zelensky, R. Kanaar, C. Wyman, Mediators of homologous DNA pairing. *Cold Spring Harb. Perspect. Biol.* **6**, a016451 (2014).
15. J. C. Bell, S. C. Kowalczykowski, Mechanics and single-molecule interrogation of DNA Recombination. *Annu. Rev. Biochem.* **85**, 193–226 (2016).
16. S. C. Kowalczykowski, An overview of the molecular mechanisms of recombinational DNA repair. *Cold Spring Harb. Perspect. Biol.* **7**, a016410 (2015).
17. P. Bork, N. Blomberg, M. Nilges, Internal repeats in the BRCA2 protein sequence. *Nat. Genet.* **13**, 22–23 (1996).
18. G. Bignell, G. Micklem, M. R. Stratton, A. Ashworth, R. Wooster, The BRC repeats are conserved in mammalian BRCA2 proteins. *Hum. Mol. Genet.* **6**, 53–58 (1997).
19. L. Pellegrini *et al.*, Insights into DNA recombination from the structure of a RAD51-BRCA2 complex. *Nature* **420**, 287–293 (2002).
20. A. Carreira *et al.*, The BRC repeats of BRCA2 modulate the DNA-binding selectivity of RAD51. *Cell* **136**, 1032–1043 (2009).
21. A. Carreira, S. C. Kowalczykowski, Two classes of BRC repeats in BRCA2 promote RAD51 nucleoprotein filament function by distinct mechanisms. *Proc. Natl. Acad. Sci. U.S.A.* **108**, 10448–10453 (2011).
22. H. Yang *et al.*, BRCA2 function in DNA binding and recombination from a BRCA2-DSS1-ssDNA structure. *Science* **297**, 1837–1848 (2002).
23. S. C. Kowalczykowski, Molecular mimicry connects BRCA2 to Rad51 and recombinational DNA repair. *Nat. Struct. Biol.* **9**, 897–899 (2002).
24. W. Zhao *et al.*, Promotion of BRCA2-dependent homologous recombination by DSS1 via RPA targeting and DNA mimicry. *Mol. Cell* **59**, 176–187 (2015).
25. G. Chatterjee, J. Jimenez-Sainz, T. Presti, T. Nguyen, R. B. Jensen, Distinct binding of BRCA2 BRC repeats to RAD51 generates differential DNA damage sensitivity. *Nucleic Acids Res.* **44**, 5256–5270 (2016).
26. A. L. Forget, C. C. Dombrowski, I. Amitani, S. C. Kowalczykowski, Exploring protein-DNA interactions in 3D using in situ construction, manipulation and visualization of individual DNA dumbbells with optical traps, microfluidics and fluorescence microscopy. *Nat. Protoc.* **8**, 525–538 (2013).
27. A. L. Forget, S. C. Kowalczykowski, Single-molecule imaging of DNA pairing by RecA reveals a three-dimensional homology search. *Nature* **482**, 423–427 (2012).
28. J. C. Bell, J. L. Plank, C. C. Dombrowski, S. C. Kowalczykowski, Direct imaging of RecA nucleation and growth on single molecules of SSB-coated ssDNA. *Nature* **491**, 274–278 (2012).
29. T. Shahid *et al.*, Structure and mechanism of action of the BRCA2 breast cancer tumor suppressor. *Nat. Struct. Mol. Biol.* **21**, 962–968 (2014).
30. J. Hilario, I. Amitani, R. J. Baskin, S. C. Kowalczykowski, Direct imaging of human Rad51 nucleoprotein dynamics on individual DNA molecules. *Proc. Natl. Acad. Sci. U.S.A.* **106**, 361–368 (2009).
31. H. Naora, H. Naora, M. Izawa, V. G. Allfrey, A. E. Mirsky, Some observations on differences in composition between the nucleus and cytoplasm of the frog oocyte. *Proc. Natl. Acad. Sci. U.S.A.* **48**, 853–859 (1962).
32. R. Galletto, I. Amitani, R. J. Baskin, S. C. Kowalczykowski, Direct observation of individual RecA filaments assembling on single DNA molecules. *Nature* **443**, 875–878 (2006).
33. A. Candelli *et al.*, Visualization and quantification of nascent RAD51 filament formation at single-monomer resolution. *Proc. Natl. Acad. Sci. U.S.A.* **111**, 15090–15095 (2014).
34. H. Yang, Q. Li, J. Fan, W. K. Holloman, N. P. Pavletich, The BRCA2 homologue Brh2 nucleates RAD51 filament formation at a dsDNA-ssDNA junction. *Nature* **433**, 653–657 (2005).
35. H. Saeki *et al.*, Suppression of the DNA repair defects of BRCA2-deficient cells with heterologous protein fusions. *Proc. Natl. Acad. Sci. U.S.A.* **103**, 8768–8773 (2006).
36. M. Spies, S. C. Kowalczykowski, The RecA binding locus of RecBCD is a general domain for recruitment of DNA strand exchange proteins. *Mol. Cell* **21**, 573–580 (2006).
37. L. S. Symington, End resection at double-strand breaks: Mechanism and regulation. *Cold Spring Harb. Perspect. Biol.* **6**, a016436 (2014).
38. J. C. Bell, S. C. Kowalczykowski, RecA: Regulation and mechanism of a molecular search engine. *Trends Biochem. Sci.* **41**, 491–507 (2016).
39. K. Morimatsu, S. C. Kowalczykowski, RecFOR proteins load RecA protein onto gapped DNA to accelerate DNA strand exchange: A universal step of recombinational repair. *Mol. Cell* **11**, 1337–1347 (2003).
40. R. B. Jensen, A. Ozes, T. Kim, A. Estep, S. C. Kowalczykowski, BRCA2 is epistatic to the RAD51 paralogs in response to DNA damage. *DNA Repair (Amst)* **12**, 306–311 (2013).
41. J. Chun, E. S. Buechelmaier, S. N. Powell, Rad51 paralog complexes BCDX2 and CX3 act at different stages in the BRCA1-BRCA2-dependent homologous recombination pathway. *Mol. Cell. Biol.* **33**, 387–395 (2013).
42. H. M. Thorpe, M. C. Smith, In vitro site-specific integration of bacteriophage DNA catalyzed by a recombinase of the resolvase/invertase family. *Proc. Natl. Acad. Sci. U.S.A.* **95**, 5505–5510 (1998).
43. I. Amitani, B. Liu, C. C. Dombrowski, R. J. Baskin, S. C. Kowalczykowski, Watching individual proteins acting on single molecules of DNA. *Methods Enzymol.* **472**, 261–291 (2010).